J. Cent. South Univ. (2021) 28: 3418−3433
DOI: https://doi.org/10.1007/s11771-021-4865-9

Springer

Thermal stress distribution around a thermally-insulated polygonal cutout in graphite/epoxy composite laminates under heat flux

Mohammad Hossein BAYATI CHALESHTARI, Hadi KHORAMISHAD*

School of Mechanical Engineering, Iran University of Science and Technology, Narmak, Tehran 16846, Iran

Abstract: In this study, the effect of influencing parameters on the stress distribution around a polygonal cutout within a laminated composite under uniform heat flux was analytically examined. The analytical method was developed based on the classical laminated plate theory and two-dimensional thermo-elastic method. A mapping function was employed to extend the solution of a perforated symmetric laminate with a circular cutout to the solution of polygonal cutouts. The effect of significant parameters such as the cutout angular position, bluntness and aspect ratio, the heat flux angle and the laminate stacking sequence in symmetric composite laminate containing triangular, square and pentagonal cutouts was studied. The Neumann boundary condition was used at the edges of the thermally insulated polygonal cutout. The laminate was made of graphite/epoxy (AS/3501) material with two different stacking sequences of $[30/45]_s$ and $[30/0/-30]_s$. The analytical solutions were well validated against finite element results.

Key words: analytical solution; thermal stress analysis; polygonal cutout; complex variable method; polymeric composite

Cite this article as: Mohammad Hossein BAYATI CHALESHTARI, Hadi KHORAMISHAD. Thermal stress distribution around a thermally-insulated polygonal cutout in graphite/epoxy composite laminates under heat flux [J]. Journal of Central South University, 2021, 28(11): 3418−3433. DOI: https://doi.org/10.1007/s11771-021-4865-9.

1 Introduction

In recent years, the use of composite plates with cutouts in various engineering industries such as aerospace industry, steam and gas turbines, shipbuilding industry and complex engineering structures has significantly increased. Such structures are likely to be subjected to thermal loading. The existence of geometric discontinuities, such as cutouts, causes disturbance in the heat flux resulting in non-uniform thermal expansion and consequently thermal stresses. Perforated multilayer composite laminates are used in various industries. Cutouts are made in composite laminates for different purposes such as for reducing the structural weight and producing man-holes. Thermal stresses can decrease the strength and lead to premature failures in structures [1, 2]. Therefore, having accurate information about thermal stress distribution around cutouts is of high importance. According to the literature [3], structures with cutout have lower strength compared to the structures without cutout and about 80% of failures in aircraft structures occur at the holes made for mechanically fastened joints [4].

Several researchers [5 − 7] have studied the stress distribution around cutouts. MUSKHELISHVILI [5] used complex potential functions for solving the 2D elastic problems.

Received date: 2020-09-22; **Accepted date:** 2021-05-10
Corresponding author: Hadi KHORAMISHAD, PhD, Associate Professor; E-mail: khoramishad@iust.ac.ir; ORCID: https://orcid.org/0000-0003-2705-0203

SAVIN [6] and LEKHNITSKII [7] were amongst the first researchers who contributed effectively in the stress analysis of anisotropic and isotropic plates with cutouts using MUSKHELISHVILI's method. SHARMA [8] applied the complex variable method to obtain a general solution for an infinite laminate with a polygonal cutout for two different layups of $[0/90]_s$ and $[45/-45]_s$. Moreover, SHARMA [9] investigated the effect of cutout geometrical parameters on the stress distribution in infinite isotropic plates under in-plane loading. He obtained the analytical solution using the complex variable technique and conformal transformation. LU et al [10] investigated stress distribution around a cutout with circular or elliptical shape in an infinite plate using an analytical method. They employed conformal mapping function to obtain the stress distribution around cutout when the plate was subjected to mechanical loading. QI et al [11] investigated the fatigue life of laminated composites containing a circular cutout. They considered the different diameters for the circular cutout.

RAO et al [12] used Savin's method to derive stress distribution around a square cutout in symmetric laminates with cross-ply, angle-ply and various stacking sequences under arbitrary biaxial mechanical loading. DAVE and SHARMA [13] studied stress distribution around a square cutout in a functionally graded plate. They used the complex variable method to obtain moment and stress under mechanical loading. MOUSANEZHAD et al [14] proposed an analytical method for determining the inter-laminar stresses in symmetric laminated composite plates subjected to shear loads. They employed first-order shear deformation theory and Reddy's layer-wise theory to determine the inter-laminar stresses in composite laminates under extension and bending loads. JAFARI and BAYATI [15] used the gray wolf optimization algorithm to achieve optimum stress in orthotropic plates containing polygonal cutouts. They applied an analytical method based on the Lekhnitskii's solution. JAFARI and BAYATI [16] determined the optimal values of the parameters affecting the normalized stress around a quasi-triangular cutout in an orthotropic plate. The design variables in this study were the loading angle, the cutout rotation angle, the fiber angle and bluntness.

Recently, thermal stress has been considered by researchers [17, 18]. The employment of complex potential function for 2D thermo-elastic problems in isotropic plate with holes was introduced by FLORENCE and GOODIER [19]. BHULLAR [20] investigated thermal stresses in a hexagonal region subject to uniform heat flux and achieved the variation of the tangential stress around a cutout. TARN and WANG [21] presented thermal stresses in an anisotropic elastic body with a rigid inclusion by the assumption of plane stress and plane strain conditions using Lekhnitskii's complex potential method. JAFARI et al [22] obtained thermal stresses around a polygonal cutout in metallic plates based on the two-dimensional thermoelastic theory under a steady-state condition. They examined the effect of parameters on the value of thermal stress for different shapes of the cutout. HASEBE et al [23] employed conformal mapping function and complex variable technique to determine thermal stress distribution in an infinite plate containing an elliptical cutout. Moreover, ZHANG et al [24] used conformal mapping function and complex variable method for two-dimensional problem of an elliptical cutout in a thermo-electric isotropic material under uniform electric current density. WANG et al [25] obtained a closed-form solution for the 2D thermo-elastic problem of an isotropic plate with an elliptical cutout using the complex variable method. HASEBE et al [26] proposed a formulation based on the two-dimensional thermo-elastic theory and used complex variable technique for an isotropic plate subjected to uniform heat flux with different thermal and mechanical boundary conditions. RASOULI and JAFARI [27] employed the conformal mapping technique and Lekhnitskii's method to obtain the thermal stress distribution around a circular or elliptical cutout in a single-layer anisotropic plate subjected to a uniform heat flux. They studied the effect of the cutout orientation and flux angle parameters on the stress distribution around cutout. CHAO et al [28] obtained a general analytical solution for thermal stresses in an anisotropic plate under uniform heat flux with elliptical inclusion. They applied the conformal mapping and Lekhnitskii's complex variable technique to solve the problem. WANG et al [29] proposed a general perturbation solution method for the 2D thermo-elastic problem of a laminate with a circular elastic inclusion of arbitrary shape using

conformal mapping function. JAFARI et al [30] studied thermal stress distribution and displacement in orthotropic plates containing a square cutout. They applied the analytical solution and complex variable method to determine the thermal stress distribution around the cutout. Furthermore, JAFARI et al [31] presented the stress distribution surrounding a noncircular cutout within an infinite composite plate under steady-state condition by utilizing the two-dimensional thermo-elastic theory.

Many studies were carried out on the circular and elliptical cutouts and relatively fewer works have been conducted on non-circular cutouts. However, researchers have addressed single-layer plates with isotropic and anisotropic properties and no one has analytically studied thermal stresses in multilayer composite plate with non-circular cutouts. In this article, the thermal stress distribution in a symmetric composite laminate with different stacking sequences containing a polygonal cutout was investigated using an analytical method based on the complex variable method. The effect of significant parameters such as the heat flux angle, the cutout angular position, bluntness and aspect ratio and the laminate stacking sequence was examined on the thermal stress distribution around a cutout with different shapes of triangular, square and pentagonal. The present study obtained an equivalent thermal conductivity for a perforated symmetric laminated composite and achieved thermal stresses using the conformal mapping technique and Lekhnitskii's method.

2 Analytical formulations

A symmetric laminate was assumed to be linearly elastic and anisotropic governed by generalized Hooke's law. The edge of the polygonal cutout was assumed to be insulated. The size of the cutout in comparison with the dimensions of the laminate was small enough so the laminate was considered infinite. The cutout angular position indicating the cutout orientation relative to the horizontal axis was represented by β. As shown in Figure 1, the laminate was subjected to a remote uniform heat flux q under steady-state condition.

The uniform heat flux was disturbed by the presence of a thermally insulated polygonal cutout

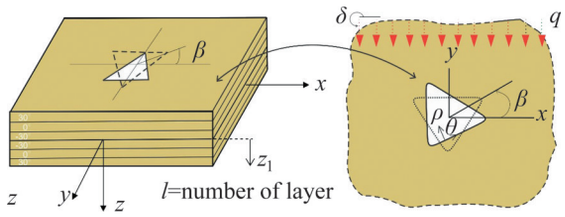

Figure 1 Symmetric composite laminate containing a quasi-triangular cutout under uniform heat flux

giving rise to thermal stresses around the cutout. Due to the absence of a heat source in the laminate, the maximum stress occurred on the edges of the cutout. Moreover, because of the boundary conditions around the cutout by considering the normal and tangential coordinate system (ρ, θ) according to Figure 1, the only stress created at the edges of cutout was σ_θ. The plane stress and small deformation conditions were assumed. According to the generalized Hooke's law, the thermal stress components can be obtained using Eq. (1) [32].

$$\{\sigma\}^{\mathrm{T}} = \{\Phi\}T \tag{1}$$

in which

$$\begin{Bmatrix}\Phi_x\\ \Phi_y\\ \Phi_{xy}\end{Bmatrix} = \frac{1}{H}\sum_{l=1}^{N}\begin{bmatrix}\bar{Q}_{11} & \bar{Q}_{12} & \bar{Q}_{16}\\ \bar{Q}_{12} & \bar{Q}_{22} & \bar{Q}_{26}\\ \bar{Q}_{16} & \bar{Q}_{26} & \bar{Q}_{66}\end{bmatrix}^{l}\begin{Bmatrix}\overline{\alpha_x}\\ \overline{\alpha_y}\\ \overline{\alpha_{xy}}\end{Bmatrix}^{l}(z_l - z_{l-1}) \tag{2}$$

where T is temperature, z_l and z_{l-1} represent the z components of the upper and lower boundaries of the lth layer, H is the total thickness and $\{\bar{\alpha}\}^l$ is the vector of the coefficient of thermal expansion of the lth layer in the global material coordinate system (off-axis) and is determined as Eq. (3).

$$\begin{cases}\overline{\alpha_x} = \alpha_{11}m^2 + \alpha_{22}n^2\\ \overline{\alpha_y} = \alpha_{11}n^2 + \alpha_{22}m^2\\ \overline{\alpha_{xy}} = 2mn(\alpha_{11} - \alpha_{22})\end{cases} \tag{3}$$

where α_{11} and α_{22} are the coefficients of thermal expansion in the local material coordinate system (on-axis). Furthermore, m and n are the corresponding cosine and sine of the fiber angle γ. According to the Likhnitskii's complex potential technique and by considering the Airy's stress function $E(x, y)$, the stress components are defined as Eq. (4). Using Eqs. (1) and (4) and the stress–strain relationship and the compatibility equation,

the constitutive equation for an anisotropic material can be obtained in terms of the stress function as Eq. (5).

$$\sigma_x = \frac{\partial^2 E}{\partial y^2}, \sigma_y = \frac{\partial^2 E}{\partial x^2}, \tau_{xy} = -\frac{\partial^2 E}{\partial x \partial y} \tag{4}$$

$$a_{11}\frac{\partial^4 E}{\partial y^4} - 2a_{16}\frac{\partial^4 E}{\partial x \partial y^3} + (2a_{12} + a_{66})\frac{\partial^4 E}{\partial x^2 \partial y^2} - 2a_{26}\frac{\partial^4 E}{\partial x^3 \partial y} + a_{22}\frac{\partial^4 E}{\partial x^4} = -\alpha_x \frac{\partial^2 T}{\partial y^2} + \alpha_{xy}\frac{\partial^2 T}{\partial x \partial y} - \alpha_y \frac{\partial^2 T}{\partial x^2} \tag{5}$$

where a_{ij} (i, j=1, 2, 6) denotes the enteries of the reduced complinance matrix of the symmetric laminate and α_x, α_y and α_{xy} are the thermal expansion coefficients in the global coordinate system and can be obtained using Eq. (6).

$$\begin{cases} \alpha_x = a_{11}\Phi_x + a_{12}\Phi_y + a_{16}\Phi_{xy} \\ \alpha_y = a_{12}\Phi_x + a_{22}\Phi_y + a_{26}\Phi_{xy} \\ \alpha_{xy} = a_{16}\Phi_x + a_{26}\Phi_y + a_{66}\Phi_{xy} \end{cases} \tag{6}$$

The solution of Eq. (5) is divided into two parts including the homogenous ($E^{(h)}$) and private ($E^{(p)}$) parts. The generalized biharmonic equation for an anisotropic material in terms of the stress function (E) is:

$$a_{11}\frac{\partial^4 E^{(h)}}{\partial y^4} - 2a_{16}\frac{\partial^4 E^{(h)}}{\partial x \partial y^3} + (2a_{12} + a_{66})\frac{\partial^4 E^{(h)}}{\partial x^2 \partial y^2} - 2a_{26}\frac{\partial^4 E^{(h)}}{\partial x^3 \partial y} + a_{22}\frac{\partial^4 E^{(h)}}{\partial x^4} = 0 \tag{7}$$

Using four first-order linear differential operators ($D_k = \frac{\partial}{\partial y} - s_k \frac{\partial}{\partial x}$), in which s_k (k=1, 2, 3, 4) are the roots of the characteristic equation (Eq. (8)). Equation (6) can be rewritten as $D_1D_2D_3D_4E^{(h)}$=0.

$$a_{11}s^4 - 2a_{16}s^3 + (2a_{12} + a_{66})s^2 - 2a_{26}s + a_{22} = 0 \tag{8}$$

The roots of Eq. (8) can be presented as Eq. (9).

$$s_1 = \alpha_1 + i\beta_1,\ s_2 = \overline{s_1} = \alpha_1 - i\beta_1,$$

$$s_3 = \alpha_2 + i\beta_2,\ s_4 = \overline{s_3} = \alpha_2 - i\beta_2 \tag{9}$$

where α_1, α_2, β_1 and β_2 are real numbers. For symmetric laminates we have $a_{16} = a_{26} = 0$. The function $E^{(h)}$ is considered as Eq. (10) in which Z_k is the mapping function.

$$E^{(h)} = 2Re\sum_{k=1}^{2} E_k(Z_k) \tag{10}$$

By substituting Eq. (10) into Eq. (7) and integrating with respect to Z_k, the function $E^{(h)}$ can be obtained and the general solution of Eq. (5) can be expressed in the form of Eq. (11).

$$E = E_1(Z_1) + E_2(Z_2) + \overline{E_1(Z_1)} + \overline{E_2(Z_2)} + E^{(p)} \tag{11}$$

where $z_k = x + s_k y$ (k = 1, 2, t), E_1 and E_2 are analytic functions and $\overline{E_1}$ and $\overline{E_2}$ are their conjugates, respectively. In order to reduce the derivative order, a new stress function (ψ) is defined. The new stress function (ψ) is derived using the stress function E as below:

$$\frac{\mathrm{d}E}{\mathrm{d}z} = \psi_1(Z_1) + \psi_2(Z_2) + \overline{\psi_1(Z_1)} + \overline{\psi_2(Z_2)} + \psi^{(p)} \tag{12}$$

Using Eqs. (4), (11) and (12), the stress components are determined as Eq. (13).

$$\begin{cases} \sigma_x = 2\mathrm{Re}\left\{s_1^2\psi_1'(Z_1) + s_2^2\psi_2'(Z_2)\right\} + \dfrac{\partial^2 E^{(p)}}{\partial y^2} \\ \sigma_y = 2\mathrm{Re}\left\{\psi_1'(Z_1) + \psi_2'(Z_2)\right\} + \dfrac{\partial^2 E^{(p)}}{\partial x^2} \\ \tau_{xy} = -2\mathrm{Re}\left\{s_1\psi_1'(Z_1) + s_2\psi_2'(Z_2)\right\} - \dfrac{\partial^2 E^{(p)}}{\partial x \partial y} \end{cases} \tag{13}$$

where $\psi_1'(Z_1)$ and $\psi_2'(Z_2)$ are the derivatives of functions $\psi_1(Z_1)$ and $\psi_2(Z_2)$ with respect to Z_1 and Z_2 , respectively. In order to relate the on-axis heat flux q and temperature gradient in an orthotropic laminate, the Fourier's law was employed in the form of Eq. (14).

$$\{q\}_{\mathrm{on}} = -[k]_{\mathrm{on}}\{\nabla T\}_{\mathrm{on}} \tag{14}$$

In Eq. (14), $[k]_{\mathrm{on}}$ is the on-axis anisotropic thermal conductivity matrix and T is the temperature change. It was assumed that the unidirectional laminas were isotropic in a plane normal to the fibers (i. e., transversely isotropic). The Fourier's law of thermal conduction in the global coordinate system can be presented as Eq. (15).

$$\{q\}_{\mathrm{off}} = [T(-\gamma)][k]_{\mathrm{on}}[T(\gamma)]\{\nabla T\}_{\mathrm{off}} \tag{15}$$

By considering n=sinγ and m=cosγ, the components of the off-axis thermal conductivity

matrix $[\bar{k}]_{\text{off}} = [\bar{k}]$ are defined as Eq. (16).

$$\bar{k}_{11} = m^2 k_{11} + n^2 k_{22}, \bar{k}_{12} = mn(k_{22} - k_{11}),$$
$$\bar{k}_{22} = n^2 k_{11} + m^2 k_{22}, \bar{k}_{13} = 0, \bar{k}_{33} = k_{22}, \bar{k}_{23} = 0 \quad (16)$$

By integrating the off-axis thermal conductivity coefficients across the laminate thickness, the resultant of thermal conductivity coefficients for a multilayer laminate can be determined using Eq. (17).

$$[K] = \int_{-H/2}^{H/2} [\bar{k}]^l \mathrm{d}z = \sum_{l=1}^{N_L} \int_{z_{l-1}}^{z_l} [\bar{k}]^l \mathrm{d}z \quad (17)$$

where $[K]$ is the thermal conductivity resultant matrix and N_L is the number of layers. Moreover, for a laminate without internal heat source or sink we have [21]

$$\nabla q_i = 0 \quad (18)$$

By substituting Eq. (15) into Eq. (18), the governing equation for temperature is expressed as Eq. (19).

$$K_x \frac{\partial^2 T}{\partial x^2} + 2K_{xy} \frac{\partial^2 T}{\partial x \partial y} + K_y \frac{\partial^2 T}{\partial y^2} = 0 \quad (19)$$

The harmonic function of $T(x, y)$ satisfying Eq. (19) can be obtained as the temperature distribution in laminate. The solution of Eq. (19) can be considered as $T=E_t(x+s_t y)$ where s_t is the root of the characteristic equation. As the thermal conductivity matrix is invertible and positive definite ($K_x K_y > K_{xy}^2$), the characteristic equation contains two complex conjugate roots. Therefore, the solution of Eq. (19) can be introduced as Eq. (20).

$$T = E_t(x + s_t y) + \overline{E_t(x + s_t y)} = 2\mathrm{Re}(E_t(x + s_t y)) \quad (20)$$

where E_t is a complex function. By substituting Eq. (20) into Eq. (5), the particular solution of the stress functions $E^{(p)}$ can be obtained. So, the stress components are obtained in terms of the stress functions as Eq. (21).

$$\begin{cases} \sigma_x = 2\mathrm{Re}\{s_1^2 \psi_1'(Z_1) + s_2^2 \psi_2'(Z_2)\} + 2\mathrm{Re}(\upsilon s_t^2 \psi_t') \\ \sigma_y = 2\mathrm{Re}\{\psi_1'(Z_1) + \psi_2'(Z_2)\} + 2\mathrm{Re}(\upsilon \psi_t') \\ \tau_{xy} = -2\mathrm{Re}\{s_1 \psi_1'(Z_1) + s_2 \psi_2'(Z_2)\} - 2\mathrm{Re}(\upsilon s_t \psi_t') \end{cases} \quad (21)$$

where υ is defined in Eq. (22).

$$\upsilon = \frac{(-\alpha_y + \alpha_{xy} s_t - \alpha_x s_t^2)}{a_{11} s_t^4 - 2a_{16} s_t^3 + (2a_{12} + a_{66}) s_t^2 - 2a_{26} s_t + a_{22}} \quad (22)$$

The boundary of the polygonal cutout is free from external load, therefore, the mechanical boundary conditions can be expressed in Eq. (23) [21].

$$L\psi + \overline{L\psi} + l\psi_t + \overline{l\psi_t} = 0 \quad (23)$$

where

$$L = \begin{bmatrix} -s_1 & -s_2 \\ 1 & 1 \end{bmatrix}, l = \begin{bmatrix} -\upsilon s_t \\ \upsilon \end{bmatrix}, \psi = \begin{bmatrix} \psi_1 \\ \psi_2 \end{bmatrix} \quad (24)$$

Because the boundary of the polygonal cutout is insulated, the Newman boundary condition can be expressed as Eq. (25).

$$\psi_t'(\xi) - \overline{\psi_t'(\xi)} = 0 \quad (25)$$

The function $\psi_t'(\xi)$ can be represented by two functions $r_t(\xi)$ and $p_t(\xi)$ that are holomorphic in the inner and outer areas of the unit circle, respectively.

$$\psi_t'(\xi) = r_t(\xi) + p_t(\xi) \quad (26)$$

The function $\psi_t'(\xi)$ can be expressed as the Laurent series in which the term ξ^{-1} exists. Consequently, by integrating the function $\psi_t'(\xi)$, the function $\psi_t(\xi)$ function contains the term $\log\xi$ as Eq. (27).

$$\psi_t(\xi) = R_t(\xi) + P_t(\xi) + \Pi \log\xi \quad (27)$$

$R_t(\xi)$ and $P_t(\xi)$ are holomorphic functions inside and outside the unit circle, respectively. Furthermore, the function $\psi(\xi)$ can be considered as Eq. (28).

$$\psi(\xi) = r(\xi) + p(\xi) + \Lambda \log\xi \quad (28)$$

where $r(\xi)$ and $p(\xi)$ are the holomorphic functions inside and outside the unit circle respectively. By substituting Eqs. (27) and (28) into Eq. (23) and multiplying it by $\frac{\mathrm{d}\sigma}{2\pi i(\sigma - \xi)}$ and applying the Cauchy integral, $\psi(\xi)$ can be obtained as Eq. (29).

$$\psi(\xi) = r(\xi) - L^{-1}\bar{L}\bar{r}(\xi^{-1}) - L^{-1} l P_t(\xi) - L^{-1}\bar{l}\bar{R}_t(\xi^{-1}) + \Lambda \log\xi \quad (29)$$

where

$$\Lambda = L^{-1}(\bar{M} - M)^{-1}(\Pi a - \overline{\Pi a}) + A^{\varphi -1}(\bar{M}^{-1} - M^{-1})^{-1}(\Pi l - \overline{\Pi l})$$
$$B = A^{\varphi} L^{-1},\ A^{\varphi} = \begin{bmatrix} b_1 & b_2 \\ d_1 & d_2 \end{bmatrix} \tag{30}$$

where L and A^{φ} are defined in Eqs. (24) and (30) and Π can be obtained using boundary conditions. When heat flux was applied to an anisotropic laminate without cutout, the thermal stress function is presented as Eq. (31).

$$\psi_t^{\infty\prime} = \frac{q(\cos\delta + \bar{s}_t \sin\delta)}{i(K_x K_y - K_{xy}^2)^{\frac{1}{2}}(s_t - \bar{s}_t)}(x + s_t y) \tag{31}$$

In the presence of a polygonal cutout, in addition to $\psi_t^{\infty\prime}$, the function $\psi_t^{M\prime}$, which is holomorphic outside the unit circle, is added to the thermal stress function. Therefore, the stress function can be expressed as Eq. (32).

$$\psi_t'(\xi) = \frac{q(\cos\delta + \bar{s}_t \sin\delta)}{i(K_x K_y - K_{xy}^2)^{\frac{1}{2}}(s_t - \bar{s}_t)} \cdot (\Delta_{1t}\xi + \Delta_{2t}\xi^{-1} + \Delta_{3t}\xi^{n} + \Delta_{4t}\xi^{-n}) + \psi_t^{M\prime}(\xi) \tag{32}$$

By comparing Eq. (32) and Eq. (26), the function $r_t(\xi)$ is obtained as Eq. (33).

$$r_t(\xi) = \frac{q(\cos\delta + \bar{s}_t \sin\delta)}{i(K_x K_y - K_{xy}^2)^{\frac{1}{2}}(s_t - \bar{s}_t)}\left(\Delta_{1t}\xi + \Delta_{3t}\xi^{n}\right) \tag{33}$$

Therefore, $\psi_t'(\xi)$ can be expressed as Eq. (34).

$$\psi_t'(\xi) = \frac{q(\cos\delta + \bar{s}_t \sin\delta)}{i(K_x K_y - K_{xy}^2)^{\frac{1}{2}}(s_t - \bar{s}_t)} \cdot \left(\Delta_{1t}\xi + \Delta_{3t}\xi^{n}\right) + \frac{q(\cos\delta + \bar{s}_t \sin\delta)}{i(K_x K_y - K_{xy}^2)^{\frac{1}{2}}(s_t - \bar{s}_t)} \cdot \left(\overline{\Delta_{1t}}\xi^{-1} + \overline{\Delta_{3t}}\xi^{-n}\right) \tag{34}$$

By integrating Eq. (34) and comparing it with Eq. (27), Π can be obtained as Eq. (35).

$$\Pi = -\Delta_{1t}\left\{\left[\frac{q(\cos\delta + \bar{s}_t \sin\delta)}{i(K_x K_y - K_{xy}^2)^{\frac{1}{2}}(s_t - \bar{s}_t)}\Delta_{2t}\right] \Big/ \left[-\frac{q(\cos\delta + \bar{s}_t \sin\delta)}{i(K_x K_y - K_{xy}^2)^{\frac{1}{2}}(s_t - \bar{s}_t)}\Delta_{1t}\right]\right\} - n\Delta_{3t}\left\{\left[\frac{q(\cos\delta + \bar{s}_t \sin\delta)}{i(K_x K_y - K_{xy}^2)^{\frac{1}{2}}(s_t - \bar{s}_t)}\Delta_{4t}\right] \Big/ \left[-\frac{q(\cos\delta + \bar{s}_t \sin\delta)}{i(K_x K_y - K_{xy}^2)^{\frac{1}{2}}(s_t - \bar{s}_t)}\Delta_{3t}\right]\right\} \tag{35}$$

As already mentioned, $\psi_t^{\infty\prime}$ expresses the thermal stress function for a laminate with no cutout. Hence, it only causes the laminate deformation and does not create stress. Thus, for the purpose of achieving thermal stresses, it is enough to compute $\psi_t^{M\prime}$. $\psi_t^{M\prime}$can be obtained as Eq. (36).

$$\psi_t^{M\prime}(\xi) = -\left\{\left[\frac{q(\cos\delta + \bar{s}_t \sin\delta)}{i(K_x K_y - K_{xy}^2)^{\frac{1}{2}}(s_t - \bar{s}_t)}\Delta_{2t}\right] \Big/ \left[-\left(\frac{q(\cos\delta + \bar{s}_t \sin\delta)}{i(K_x K_y - K_{xy}^2)^{\frac{1}{2}}(s_t - \bar{s}_t)}\Delta_{1t}\right)\right]\xi^{-1}\right\} - \left\{\left[\frac{q(\cos\delta + \bar{s}_t \sin\delta)}{i(K_x K_y - K_{xy}^2)^{\frac{1}{2}}(s_t - \bar{s}_t)}\Delta_{4t}\right] \Big/ \left[-\left(\frac{q(\cos\delta + \bar{s}_t \sin\delta)}{i(K_x K_y - K_{xy}^2)^{\frac{1}{2}}(s_t - \bar{s}_t)}\Delta_{3t}\right)\right]\xi^{-n}\right\} \tag{36}$$

By integrating Eq. (36) and comparing the result with Eq. (27), the functions $R_t(\xi)$ and $P_t(\xi)$ can be determined. Therefore, $\psi(\xi)$ can be obtained using Eq. (29). Finally, the stress components are achieved using Eq. (21).

To extend the analytical solution of a circular cutout to a polygonal cutout and to utilize the Cauchy integral formula, the infinite area outside the polygonal cutout was mapped to the outside area of a unite circle, as illustrated in Figure 2 [15].

Applying the Euler's relation, the conformal mapping function for a polygonal cutout can be obtained as Eq. (37).

$$z_k = w(\xi) = \frac{\lambda}{2}(\Delta_{1k}\xi + \Delta_{2k}\xi^{-1} + \Delta_{3k}\xi^{n} + \Delta_{4k}\xi^{-n}) \tag{37}$$

in which Δ_{ik}, (i=1, 2, 3, 4) are as below:

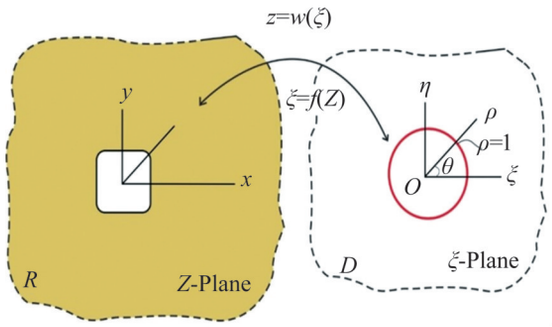

Figure 2 Conformal mapping

$$\Delta_{1k}=\frac{\lambda}{2}\left[(1-ics_k)\cos\beta-(ic+s_k)\sin\beta\right],$$

$$\Delta_{2k}=\frac{\lambda}{2}\left[(1+ics_k)\cos\beta+(ic-s_k)\sin\beta\right],$$

$$\Delta_{3k}=\frac{\lambda w}{2}\left[(1+is_k)\cos\beta+(i-s_k)\sin\beta\right],$$

$$\Delta_{4k}=\frac{\lambda w}{2}\left[(1-is_k)\cos\beta-(i+s_k)\sin\beta\right] \tag{38}$$

In Eq. (38), the parameter λ, which is positive and real, controls the size of the cutout, c determines the aspect ratio of the cutout, w determines the cutout corner curvatures (bluntness parameter) and n determines the geometry of cutout. Because the value of λ has no effect on the thermal stress distribution around the cutout, hence we can assume λ=1. The conditions $0\leqslant w<1/n$ ensure that the cutout shape does not have loops. Figure 3 shows the effect of the parameters n and w on the shape of cutout. Equation (39) is applied to model the cutout angular position (β).

$$\begin{Bmatrix}X\\Y\end{Bmatrix}=\begin{bmatrix}\cos\beta & \sin\beta\\ -\sin\beta & \cos\beta\end{bmatrix}\begin{Bmatrix}x\\y\end{Bmatrix},$$

$$x=\lambda(\cos\theta+w\cos(n\theta)),$$

$$y=\lambda(c\sin\theta-w\sin(n\theta)) \tag{39}$$

in which x and y represent the Cartesian coordinates in the laminate with polygonal cutout.

3 Validation of analytical solution

The ABAQUS finite element code was utilized to validate the proposed analytical solution. The three-dimensional models of the composite laminates with polygonal cutouts under uniform heat flux were developed. The laminates were modeled using the four-noded quadrilateral (S4R) elements. A mesh sensitivity analysis was undertaken to ensure the independence of the numerical results to the element size. The region around the cutout was modeled using fine mesh. For the mesh sensitivity analysis, the number of elements was increased from 40 to 360 and it was observed that further refining the mesh did not change the results. The numerical and analytical stress distributions (σ_θ) around the triangular, square and pentagonal cutouts were compared for two different stacking sequences of $[30/45]_s$ and $[30/0/-30]_s$ for graphite/epoxy (AS/3501) material in Figure 4. The parameter θ determines the angular position on the cutout border in relation to the horizontal axis. Figure 4 presents a reasonable correlation between the analytical and numerical results. The mechanical properties of graphite/epoxy (AS/3501) material used in this study are presented in Table 1.

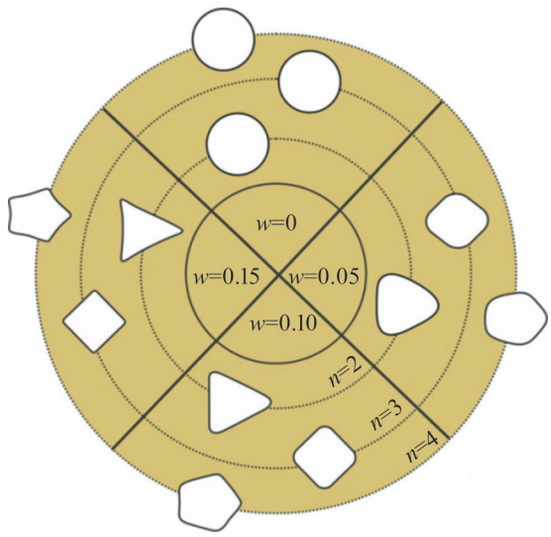

Figure 3 Effect of parameters n and w on shape of cutouts

To further validate the analytical solution, the results of the present analytical solution were compared with those presented by JAFARI et al [22] and RASOULI and JAFARI [27] in Figure 5. Figure 5(a) shows the results for an infinite isotropic plate with quasi-square cutout under uniform heat flux and Figure 5(b) represents the results for c with circular cutout subjected to uniform heat flux. Figure 5 shows good correlation between the results of the proposed analytical solution and the resuts of other researchers. To reproduce the results of

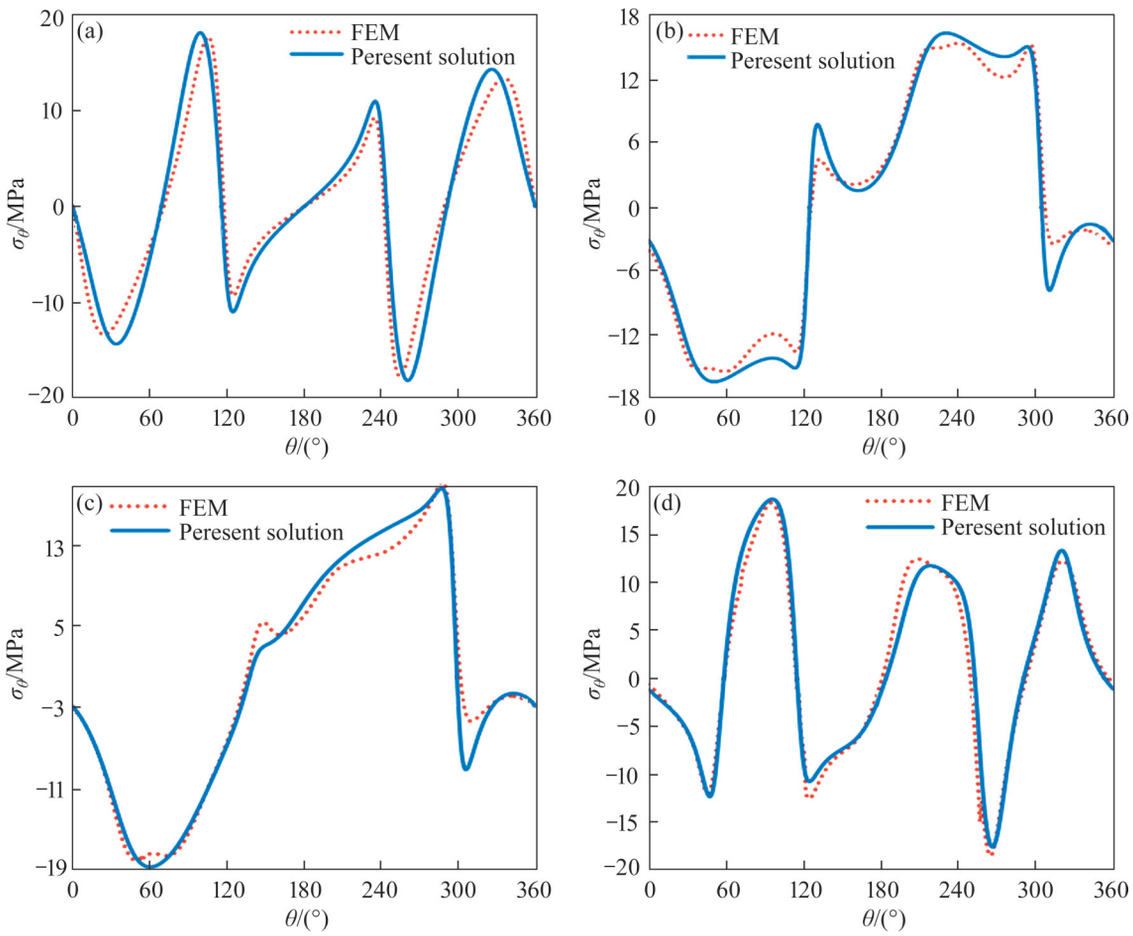

Figure 4 Comparison between analytical and numerical thermal stress distribution around (a) quasi-triangular cutout, (b) quasi-square cutout, (c) quasi-triangular cutout and (d) quasi-pentagonal cutout: (a)$[30/0/-30]_s$ lay-up, δ=270°, c=1, β=0°, w=0.125; (b) $[30/45]_s$ lay-up, δ=270°, c=1, β=30°, w=0.05; (c) $[30/45]_s$ lay-up, δ=270°, c=1, β=45°, w=0.1; (d) $[30/0/-30]_s$ lay-up, δ=270°, c=1, β=45°, w=0.05

Table 1 Materials properties of composite laminated

Material	E_{11}/GPa	E_{22}/GPa	G_{12}/GPa	υ_{12}	α_{11}/K^{-1}	A_{22}/K^{-1}	K_{11}/(W·m^{-1}·K^{-1})	K_{22}/(W·m^{-1}·K^{-1})
Graphite/epoxy (AS/3501)	144.8	9.7	4.1	0.3	-3×10^{-6}	2.8×10^{-5}	4.62	0.72

Note: $E_{33}=E_{22}$, $G_{12}=G_{13}=G_{23}$, $\upsilon_{12}=\upsilon_{13}=\upsilon_{23}$, $\alpha_{33}=\alpha_{22}$, $K_{33}=K_{22}$, $K_{12}=0$.

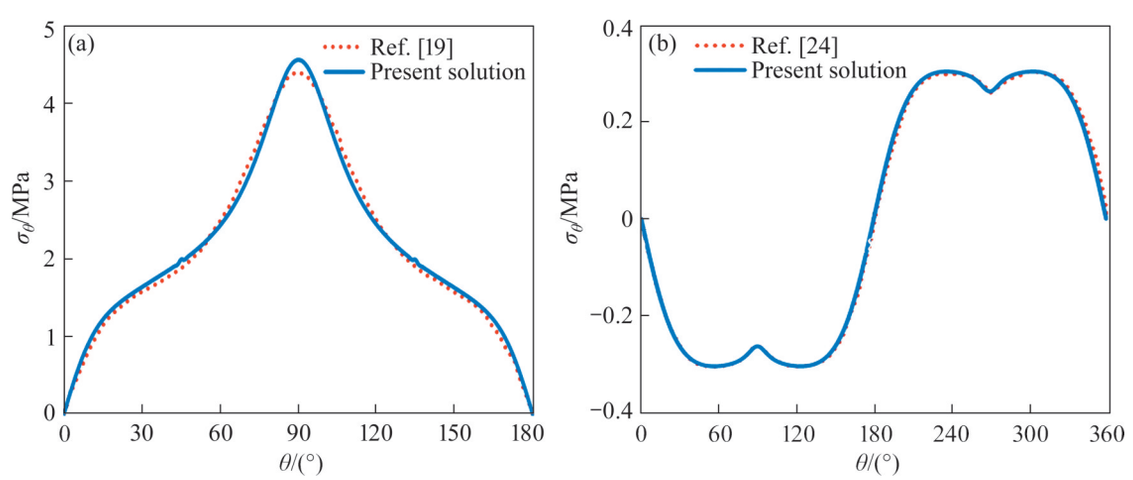

Figure 5 Comparison between present solution and Ref. [19] (a) and Ref. [24] (b)

Ref. [19], the mechanical properties of an isotropic material were considered and the number of layers was considered one. To reproduce the results of Ref. [24], the mechanical properties were considered anisotropic and the number of layers was also one. As in both references, a single-layer plate was considered, the thermal conductivity resultant matrix, defined in Eq. (17), was simplified and equal to that of a single layer.

4 Results and discussion

The thermal stress distributions around a polygonal cutout within a symmetric composite laminate were obtained using the proposed analytical method. The effects of different geometrical parameters of cutout and the laminate stacking sequence were studied on the maximum thermal stress value around cutout. The normalized maximum thermal stress is defined as $\sigma_{\text{norm}} = \dfrac{\sigma_{\theta,\max} \times k_x}{A(1,1)q_0\lambda\left|\alpha_x\right|}$ in which $\sigma_{\theta,\max}$ is the maximum circumferential stress induced around the cutout. The composite laminates made of graphite/epoxy (AS/3501) material with two stacking sequences were considered for investigation. Among the studied eases in each section, the minimum and maximum values of σ_{norm} were called desirable and undesirable thermal stresses, respectively. It should be noted that the default values of the parameters for δ, β and c were 270, 0 and 1, respectively, unless the parameters were varied in order to study their effect on the thermal stress value.

4.1 Effect of cutout angular position

The angular position of cutout is one of the effective parameters on the thermal stress distribution surrounding a polygonal cutout. Figures 6–8 show the effect of cutout angular position (β) within a laminate with different stacking sequences on the maximum normalized thermal stress for different cutout shapes of triangular, square and pentagonal, respectively, with different cutout bluntness (w) values. As can be seen in Figures 6–8, by increasing the value of w, the thermal stresses were increased. According to Figure 6, for the stacking sequence of $[30/45]_s$, the desirable and undesirable normalized thermal stresses occurred surrounding a triangular cutout at the angles of approximately 35°–50° (95°–110°) and 0°–25° (65°–95°), respectively. Whereas, for the stacking sequence of $[30/0/-30]_s$, the desirable and undesirable normalized thermal stress occurred at the angles of approximately 0°, 60°,120° and 30°, 90°, respectively.

However, as can be seen in Figure 7, for a square cutout within a laminate with a stacking sequence of $[30/45]_s$, the desirable normalized thermal stress value was obtained at a cutout angular position in the range of 25°–35° and the undesirable normalized thermal stress value was obtained at the angles of 0° and 90°. It can be seen that for the stacking sequence of $[30/45]_s$, the desirable thermal stress for w=0.075 was obtained 0.42 at β=30° while for w=0.125 was achieved 0.52 at β=40°. Furthermore, for the stacking sequence of $[30/0/-30]_s$, the desirable normalized thermal stress value was attained at 0° and 90° and the undesirable

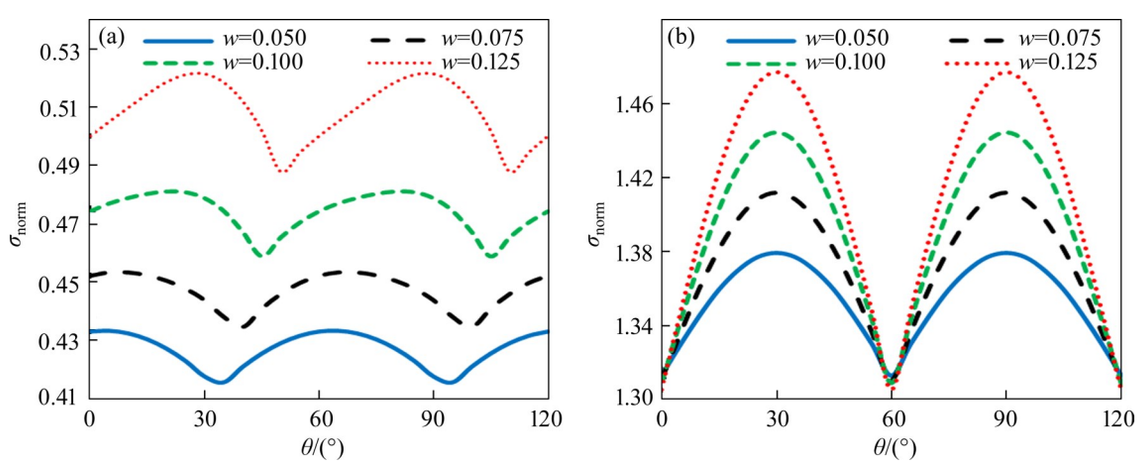

Figure 6 Effect of cutout angular position on maximum normalized thermal stress around triangular cutout for different values of w: (a) $[30/45]_s$ stacking sequence; (b) $[30/0/-30]_s$ stacking sequence

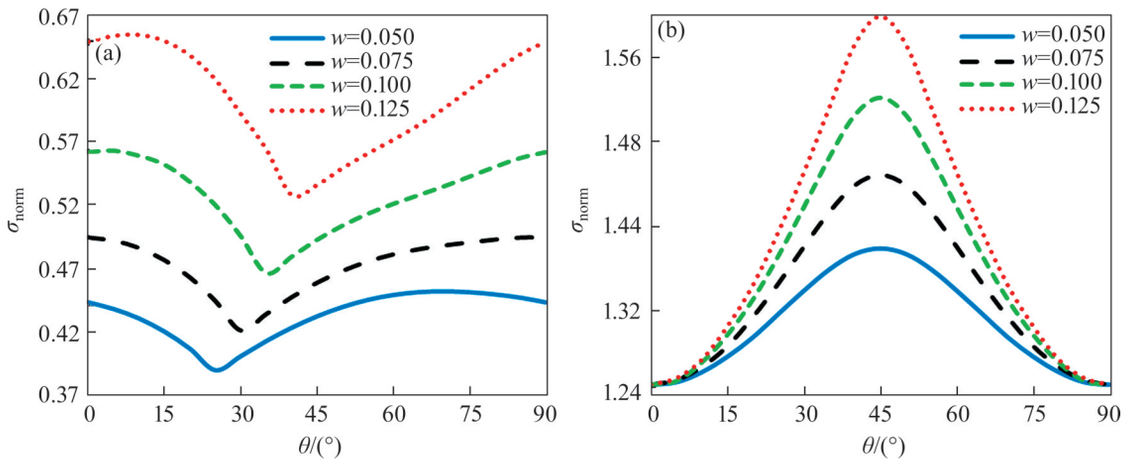

Figure 7 Effect of cutout angular position on the maximum normalized thermal stress around square cutout for different values of w: (a) $[30/45]_s$, stacking sequence; (b) $[30/0/-30]_s$, stacking sequence

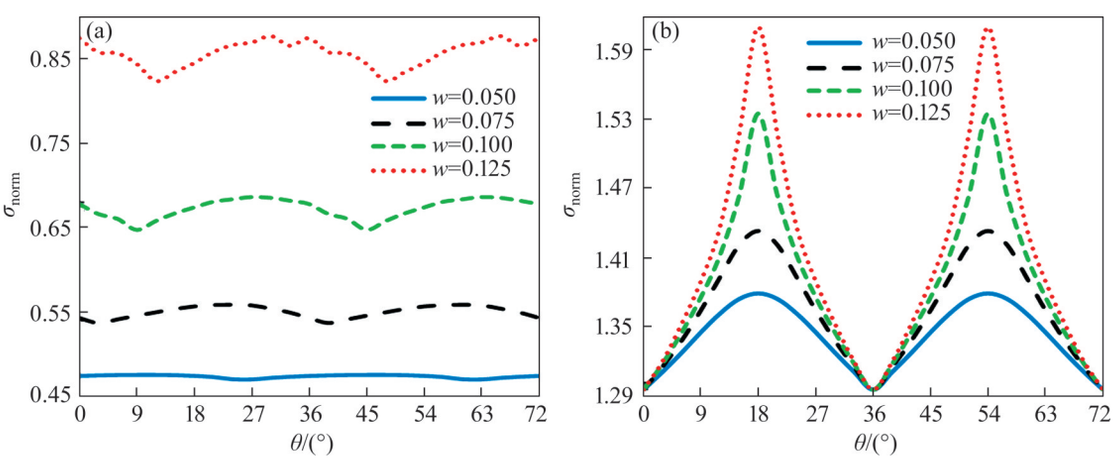

Figure 8 Effect of cutout angular position on the maximum normalized thermal stress around pentagonal cutout for different values of w: (a) $[30/45]_s$, stacking sequence; (b) $[30/0/-30]_s$, stacking sequence

normalized thermal stress value was obtained at β= 45° . Hence, the value of cutout rotation angle is important in determining the desirable and undesirable thermal stresses.

Figure 8 demonstrates the effect of cutout angular position on the normalized thermal stress distribution around the pentagonal cutout for two different stacking sequences of $[30/45]_s$ and $[30/0/-30]_s$. As shown in Figure 8, for the stacking sequence of $[30/45]_s$, by changing the bluntness parameter, the cutout angular position corresponding to the desirable thermal stress value was changed. Therefore, depending on the cutout bluntness, it is possible to adjust the cutout angular position to obtain a minimum σ_{norm} for the cutout. Moreover, as can be seen in Figure 8, for a pentagonal cutout within a laminate with a stacking sequence of $[30/45]_s$, the desirable normalized thermal stress value was obtained at a cutout angular position in the range of 3° − 12° and the undesirable normalized thermal stress value was obtained at a cutout angular position in the range of 24° − 30° . It can be seen, the maximum thermal stresses for the stacking sequence of $[30/45]_s$ for w=0.075 was 0.559 at β=24° while for w=0.1 was 0.686 at β =27° . For the stacking sequence of $[30/0/-30]_s$, the desirable normalized thermal stress value was attained at β =0° , 36° and 72° and the undesirable normalized thermal stress value was obtained at β=18° and 54° . Furthermore, amongst the cases studied, the maximum value of thermal stress was obtained for the stacking sequence of $[30/0/-30]_s$.

Table 2 presents the values of the normalized thermal stresses in the laminates with different stacking sequences containing a polygonal cutout

with different bluntness values. According to Table 2, the normalized thermal stress was dependent on the cutout bluntness parameter.

Table 2 Normalized thermal stress around a polygonal cutout for different bluntness

Stacking sequence	Triangular cutout (β=30°)		Square cutout (β=45°)		Pentagonal cutout (β=18°)	
	w	σ_{norm}	w	σ_{norm}	w	σ_{norm}
$[30/45]_s$	0	0.4019	0	0.4019	0	0.4019
	0.05	0.4176	0.05	0.4326	0.05	0.4748
	0.10	0.4788	0.10	0.493	0.10	0.6741
	0.15	0.5723	0.15	0.6107	0.15	1.1131
$[30/0/-30]_s$	0	1.3147	0	1.3147	0	1.3147
	0.05	1.3797	0.05	1.3795	0.05	1.3793
	0.10	1.4447	0.10	1.5225	0.10	1.5351
	0.15	1.5098	0.15	1.6423	0.15	1.6815

Figure 9 presents the thermal stress distributions within different layers of the $[30/45]_s$ laminate around different polygonal cutouts with different cutout angular positions under uniform heat flux and w=0.1. According to Figure 9, the 30° lamina experienced more than double thermal stress level compared to the 45° lamina, irrespective of the cutout geometry and angular position within the $[30/45]_s$ laminate made of graphite/epoxy (AS/3501). According to Figure 9, for the triangular cutout, the maximum thermal stresses for the 30° and 45° layers were obtained at β=30°, θ=244° and at β=0°, θ=235°, respectively. Also, it can be seen that for the square cutout, the maximum thermal stresses for the 30° layer were obtained at β=0°, θ=274°. Whereas, for the 45° layer the maximum thermal stresses were obtained at β=45°, θ=181°. Furthermore, the maximum thermal stresses for the 30° and 45° layers of the pentagonal cutout were obtained at β=45°, θ=221° and at β=45°, θ=79°, respectively. It should be noted that the results related to hexagonal, heptagonal cutouts and over eight sides were very similar to the results of pentagonal cutout and results were not presented.

4.2 Effect of heat flux angle

Another parameter that can influence the thermal stress distribution around the polygonal cutout in symmetric composite laminates under uniform heat flux is the heat flux angle (δ). Figures 10–12 show the effect of heat flux angle within a laminate with different stacking sequences on the maximum normalized thermal stress for different cutout shapes of triangular, square and pentagonal, respectively, with different cutout bluntness (w) values. As seen in Figure 10, the heat flux angles at which the desirable and undesirable σ_{norm} values were obtained were not dependent on the cutout bluntness value. For the stacking sequence of $[30/45]_s$, the desirable and undesirable normalized thermal stress values were obtained at the angles of approximately 125°, 305° and 40°, 220°, respectively, whereas, for the stacking sequence of $[30/0/-30]_s$, the desirable and undesirable normalized thermal stress values were obtained at the angles of 70°, 110°, 250°, 290° and 30°, 150°, 210°, 330°, respectively.

Figure 11 illustrates the effect of heat flux angle on the normalized maximum thermal stress value in the laminates with different stacking sequences of $[30/45]_s$ and $[30/0/-30]_s$ containing a square cutout with different bluntness values. As can be observed in Figure 11(a), for the stacking sequence of $[30/45]_s$, the desirable normalized thermal stress obtained at the angle of approximately 125° and 305° and the undesirable normalized thermal stress occurred at the angle of approximately 60° and 240°. According to Figure 11(b), for the stacking sequence of $[30/0/-30]_s$, the desirable normalized thermal stress occurred in the range of 80°–100° and 260°–280°. In addition, the maximum thermal stresses for the stacking sequences of $[30/45]_s$ and $[30/0/-30]_s$ were 0.732 and 1.824 at w=0.125, respectively.

Figure 12 presents the results for the pentagonal cutout. As observed in Figure 12(a), for the stacking sequence of $[30/45]_s$, the desirable normalized thermal stress occurred at the angles of approximately 125° and 305° and the undesirable normalized thermal stress occurred at the angles of approximately 60° and 240°. Furthermore, in Figure 12(b), for the stacking sequence of $[30/0/-30]_s$, the desirable normalized thermal stress occurred at the heat flux angles of 90° and 270°. Moreover, the undesirable normalized thermal stress occurred at the angles of approximately 30°, 150°, 210° and 330°.

The cutout aspect ratio (c), can also influence

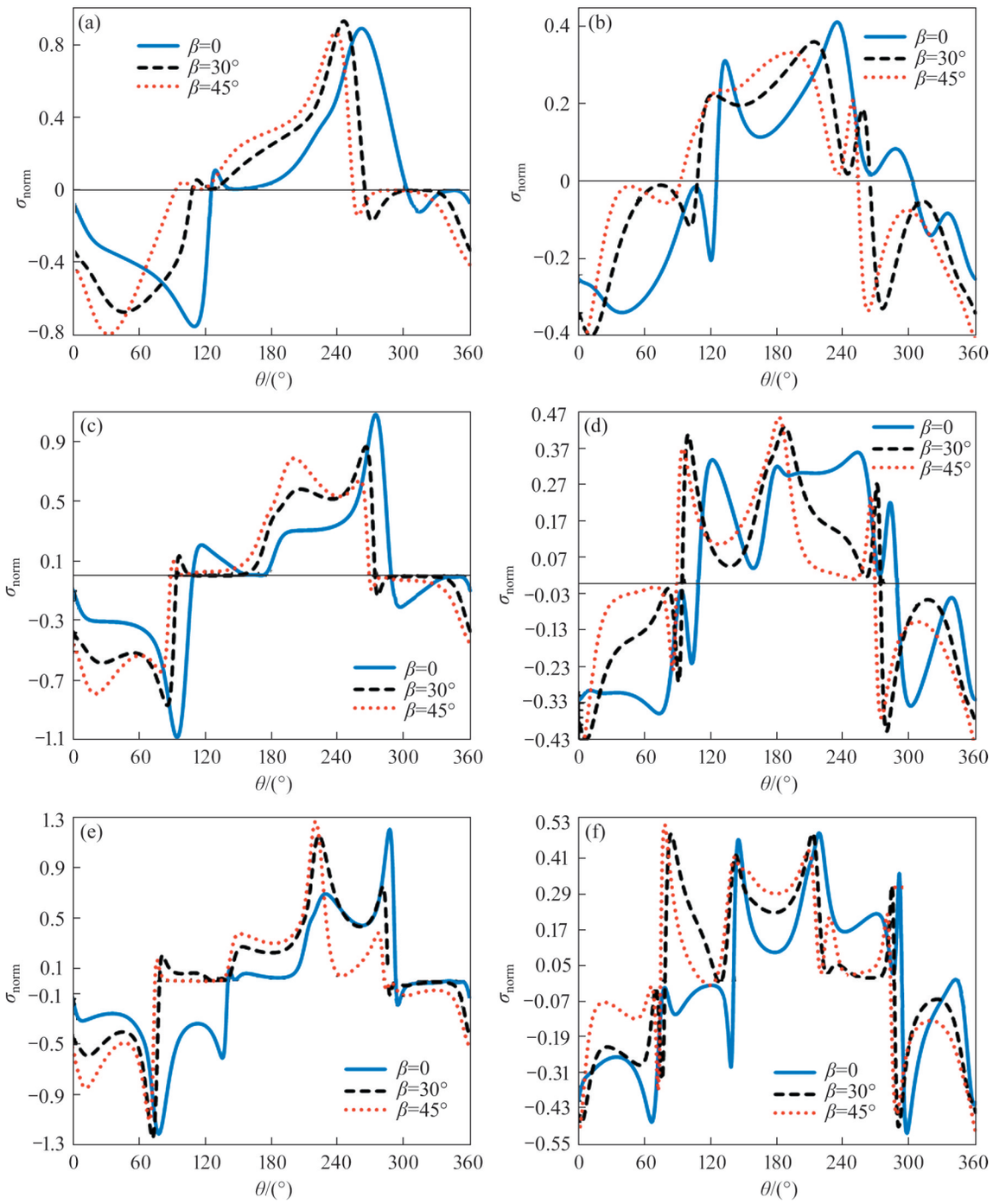

Figure 9 Thermal stress distributions within different layers of $[30/45]_s$ laminate around different polygonal cutouts with different cutout angular positions under uniform heat flux and w=0.1

the thermal stress distribution induced in a perforated laminate. Table 3 lists the values of normalized thermal stress in the laminates with different stacking sequences containing a polygonal cutout with different cutout aspect ratios. According to Table 3, for the stacking sequences of $[30/45]_s$ and $[30/0/-30]_s$, the desirable thermal stress values obtained at c=1 and c=0.5, respectively. In fact, for the stacking sequence of $[30/45]_s$, by increasing the cutout aspect ratio, initially σ_{norm} was decreased up to c=1 and afterward, it was increased. However, the trend of varying σ_{norm} with the cutout aspect ratio for the stacking sequence of $[30/0/-30]_s$ was continuously increased. It should be noted that the undesirable stress for all cutout geometry occurred at c=2.5. In design, the effective parameters should

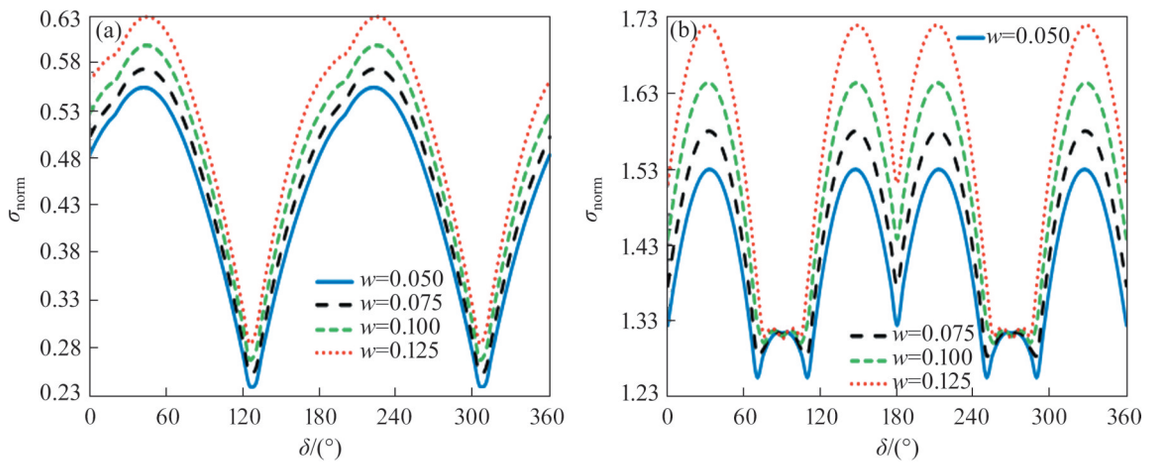

Figure 10 Effect of heat flux angle on σ_{norm} around triangular cutout for two stacking sequences for different values of w: (a) $[30/45]_s$, stacking sequence; (b) $[30/0/-30]_s$, stacking sequence

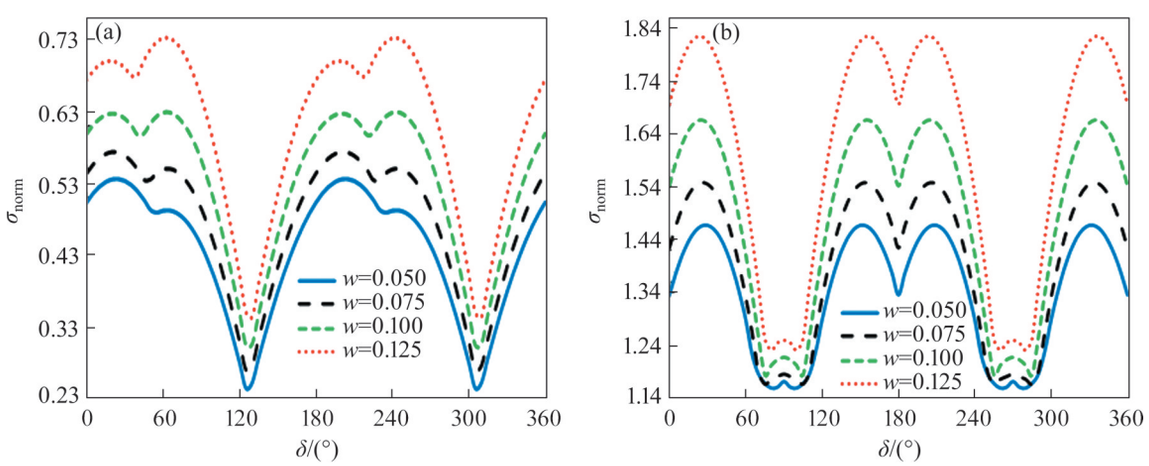

Figure 11 Effect of heat flux angle on σ_{norm} around square cutout for two stacking sequences for different values of w: (a) $[30/45]_s$, stacking sequence; (b) $[30/0/-30]_s$, stacking sequence

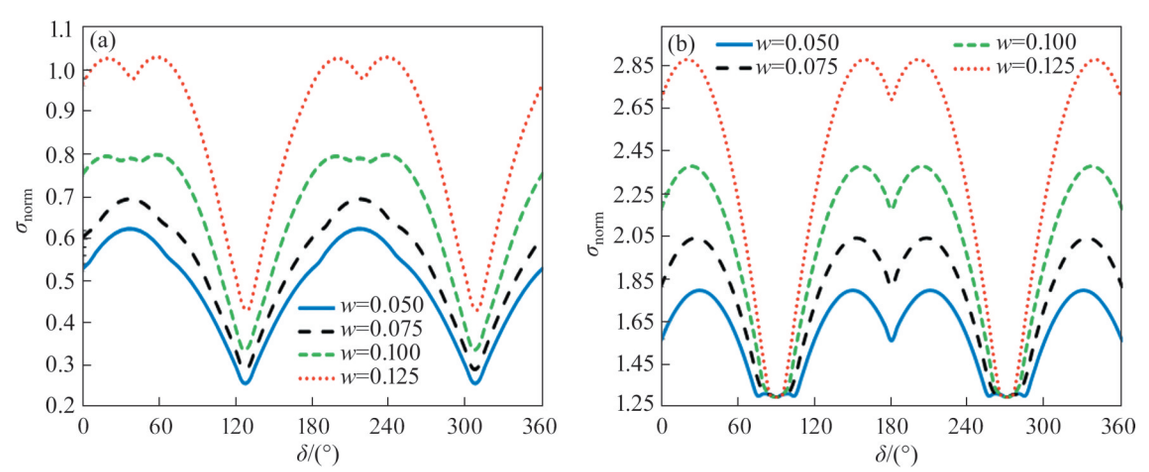

Figure 12 Effect of heat flux angle on σ_{norm} around pentagonal cutout for two stacking sequences for different values of w: (a) $[30/45]_s$, stacking sequence; (b) $[30/0/-30]_s$, stacking sequence

be chosen so the undesirable normalized thermal stress can be avoided. Figure 13 illustrates the thermal stress distributions surrounding a polygonal cutout in the laminated composites made of graphite/epoxy (AS/3501) material and different stacking sequences.

Table 3 Normalized thermal stress around a polygonal cutout for different cutout aspect ratios

Material	c	Triangular cutouts		Square cutout		Pentagonal cutout	
		$[30/45]_s$	$[30/0/-30]_s$	$[30/45]_s$	$[30/0/-30]_s$	$[30/45]_s$	$[30/0/-30]_s$
		σ_{norm}	σ_{norm}	σ_{norm}	σ_{norm}	σ_{norm}	σ_{norm}
Graphite/epoxy (AS/3501)	0.5	0.4820	1.3012	0.9136	1.1861	1.6999	1.2479
	1	0.4743	1.3094	0.5622	1.1870	0.6780	1.2515
	1.5	0.5051	1.3133	0.6978	1.1886	0.7955	1.2665
	2	0.5678	1.3169	0.8467	1.1911	0.9119	1.2743
	2.5	0.6524	1.3209	1.0001	1.1936	1.0268	1.2823

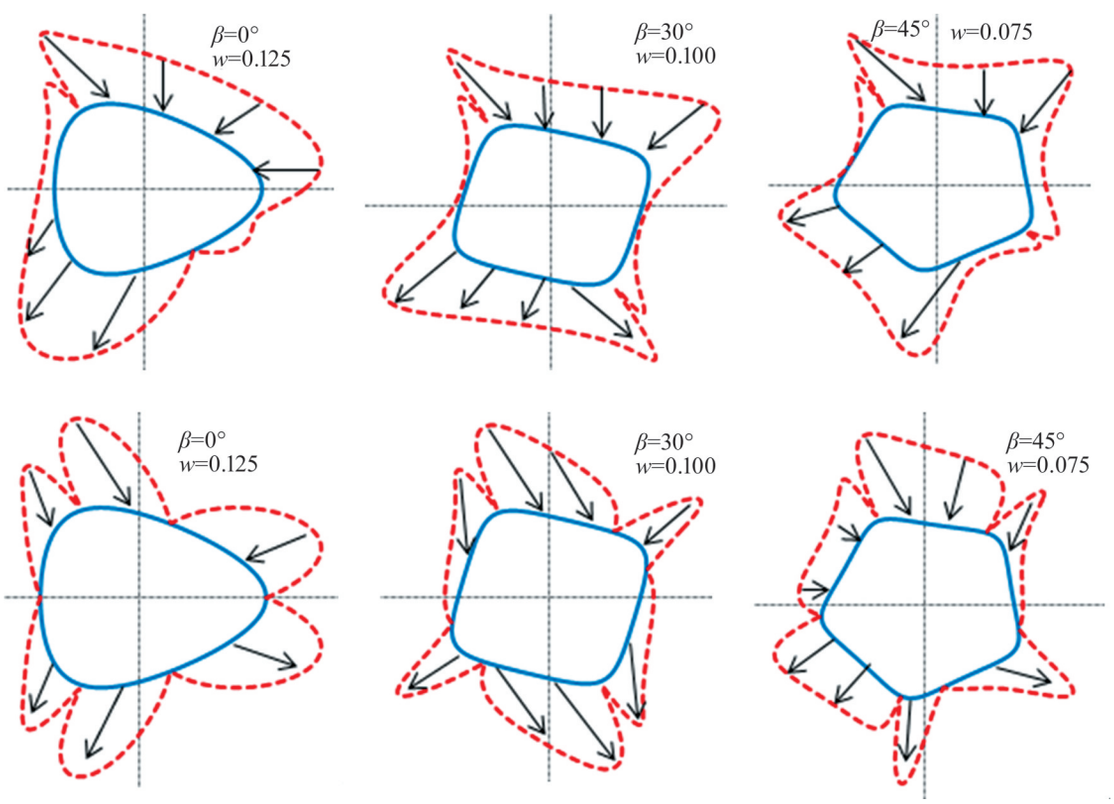

Figure 13 Thermal stress distributions surrounding a polygonal cutout with different values of w and β in laminated composites made of graphite/epoxy (AS/3501) material and different stacking sequences

5 Conclusions

Uniform heat flux can produce thermal stresses on perforated symmetric composite laminates, hence for appropriate design of industrial structures, determining the amount of thermal stress distribution around cutout is important. In this paper, the effect of influencing parameters on thermal stress distribution in a composite laminate containing a polygon cutout was analyzed using an analytical method based on the complex variable technique. The Leknitskii's method for circular and elliptical cutouts was extended to triangular, square and pentagonal cutout geometries utilizing complex variable mapping. This complex variable method can be applied in modeling and evaluation of thermal stress distribution in perforated symmetric composite laminates. The results showed that the thermal stress distribution around the cutout can be significantly dependent on the cutout shape, bluntness and angular position and the heat flux angle. According to the analytical results for all polygonal cutouts, by increasing the value of bluntness parameter (w), the desirable and undesirable stresses were increased. As observed in

the effect of the aspect ratio of cutout size parameter, the desirable thermal stress distribution for the stacking sequences of $[30/45]_s$ and [30/0/−30]s was achieved at c=1 and c=0.5, respectively. Hence, in designing perforated symmetric composite laminates, the cutout geometry should be taken into consideration so that the maximum stresses induced by uniform heat flux can be minimized.

Contributors

Mohammad Hossein BAYATI CHALESHTARI conducted the analyses and provided the first draft of manuscript. Hadi KHORAMISHAD supervised the research and edited the manuscript. All authors replied to reviewers' comments and revised the final version.

Conflict of interest

Mohammad Hossein BAYATI CHALESHTARI and Hadi KHORAMISHAD declare that they have no conflict of interest.

References

[1] LANG Lin, ZHU Zhe-ming, WANG Han-bing, HUANG Jian-wei, WANG Meng, ZHANG Xian-shang. Effect of loading rates on crack propagating speed, fracture toughness and energy release rate using single-cleavage trapezoidal open specimen under impact loads [J]. Journal of Central South University, 2020, 27(8): 2440 − 2454. DOI: 10.1007/s11771-020-4460-5.

[2] QIAN Hai, ZHOU Ding, LIU Wei-qing, FANG Hai. Elasticity solution of laminated beams subjected to thermo-loads [J]. Journal of Central South University, 2015, 22(6): 2297−2305. DOI: 10.1007/s11771-015-2754-9.

[3] GAO Chong-yang, XIAO Jian-zhang, KE Ying-lin. FE analysis of stress concentrations in composite plates with multiple holes for zigzag multi-fastened joints [J]. Materials Science Forum, 2013, 770: 17 − 20. DOI: 10.4028/www.scientific.net/msf.770.17.

[4] DEVARAJAN B, KAPANIA R K. Thermal buckling of curvilinearly stiffened laminated composite plates with cutouts using isogeometric analysis [J]. Composite Structures, 2020, 238: 111881. DOI: 10.1016/j. compstruct. 2020.111881.

[5] MUSKHELISHVILI N I. Basic equations of the plane theory of elasticity[M]//Some Basic Problems of the Mathematical Theory of Elasticity. Dordrecht: Springer Netherlands, 1977: 89−104. DOI: 10.1007/978-94-017-3034-1_4.

[6] SAVIN G N. Stress distribution around holes [M]. New York: 1961.

[7] LEKHNITSKII S G. Anisotropic plates [M]. New York: 1969. https://doi.org/0677206704.

[8] SHARMA D S. Stresses around polygonal hole in an infinite laminated composite plate [J]. European Journal of Mechanics-A/Solids, 2015, 54: 44 − 52. DOI: 10.1016/j.euromechsol.2015.06.004.

[9] SHARMA D S. Stresses around hypotrochoidal hole in infinite isotropic plate [J]. International Journal of Mechanical Sciences, 2016, 105: 32 − 40. DOI: 10.1016/j.ijmecsci.2015.10.018.

[10] LU Ai-zhong, XU Zhen, ZHANG Ning. Stress analytical solution for an infinite plane containing two holes [J]. International Journal of Mechanical Sciences, 2017, 128 − 129: 224−234. DOI: 10.1016/j.ijmecsci.2017.04.025.

[11] QI Hong-yu, WEN Wei-dong, XUN Lian-wen. Fatigue life prediction and experiment research for composite laminates with circular hole [J]. Journal of Central South University of Technology, 2004, 11(1): 19 − 22. DOI: 10.1007/s11771-004-0004-7.

[12] NAGESWARA RAO D K, RAMESH BABU M, RAJA NARENDER REDDY K, SUNIL D. Stress around square and rectangular cutouts in symmetric laminates [J]. Composite Structures, 2010, 92(12): 2845 − 2859. DOI: 10.1016/j.compstruct.2010.04.010.

[13] DAVE J M, SHARMA D S. Stress field around rectangular hole in functionally graded plate [J]. International Journal of Mechanical Sciences, 2018, 136: 360 − 370. DOI: 10.1016/j.ijmecsci.2017.12.010.

[14] MOUSANEZHAD VIYAND D, YAZDANI SARVESTANI H, NOSIER A. Stress analysis in symmetric composite laminates subjected to shearing loads [J]. International Journal of Mechanical Sciences, 2013, 75: 16 − 25. DOI: 10.1016/j.ijmecsci.2013.06.010.

[15] JAFARI M, CHALESHTARI M H B. Optimum design of effective parameters for orthotropic plates with polygonal cut-out [J]. Latin American Journal of Solids and Structures, 2017, 14(5): 906−929. DOI: 10.1590/1679-78253437.

[16] JAFARI M, BAYATI CHALESHTARI M H. Using dragonfly algorithm for optimization of orthotropic infinite plates with a quasi-triangular cut-out [J]. European Journal of Mechanics-A/Solids, 2017, 66: 1 − 14. DOI: 10.1016/j.euromechsol.2017.06.003.

[17] SHINDE B M, SAYYAD A S. Thermoelastic analysis of laminated composite and sandwich shells considering the effects of transverse shear and normal deformations [J]. Journal of Thermal Stresses, 2020, 43(10): 1234−1257. DOI: 10.1080/01495739.2020.1786484.

[18] MANTHENA V R, SRINIVAS V B, KEDAR G D. Analytical solution of heat conduction of a multilayered annular disk and associated thermal deflection and thermal stresses [J]. Journal of Thermal Stresses, 2020, 43(5): 563 − 578. DOI: 10.1080/01495739.2020.1735975.

[19] FLORENCE A L, GOODIER J N. Thermal stresses due to disturbance of uniform heat flow by an insulated ovaloid hole [J]. Journal of Applied Mechanics, 1960, 27(4): 635 − 639. DOI: 10.1115/1.3644074.

[20] BHULLAR S K, WEGNER J L. Thermal stresses in a plate with hyperelliptical hole [J]. Journal of Engineering and Technology Research, 2009, 1: 152 − 170. https://doi. org/10.5897/JETR. 9000096.

[21] TARN J Q, WANG Y M. Thermal stresses in anisotropic bodies with a hole or a rigid inclusion [J]. Journal of Thermal

Stresses, 1993, 16(4): 455−471. DOI: 10.1080/01495739308946240.
[22] JAFARI M, NAZARI M B, TAHERINASAB A. Thermal stress analysis in metallic plates with a non-circular hole subjected to uniform heat flux [J]. European Journal of Mechanics-A/Solids, 2016, 59: 356 − 363. DOI: 10.1016/j.euromechsol.2016.05.004.
[23] HASEBE N, BUCHER C, HEUER R. Heat conduction and thermal stress induced by an electric current in an infinite thin plate containing an elliptical hole with an edge crack [J]. International Journal of Solids and Structures, 2010, 47(1): 138−147. DOI: 10.1016/j.ijsolstr.2009.09.023.
[24] ZHANG A B, WANG B L. Explicit solutions of an elliptic hole or a crack problem in thermoelectric materials [J]. Engineering Fracture Mechanics, 2016, 151: 11 − 21. DOI: 10.1016/j.engfracmech.2015.11.013.
[25] WANG P, WANG B L. Thermoelectric fields and associated thermal stresses for an inclined elliptic hole in thermoelectric materials [J]. International Journal of Engineering Science, 2017, 119: 93−108. DOI: 10.1016/j.ijengsci.2017.06.018.
[26] HASEBE N, WANG Xian-feng. Complex variable method for thermal stress problem [J]. Journal of Thermal Stresses, 2005, 28(6, 7): 595−648. DOI: 10.1080/01495730590932706.
[27] RASOULI M, JAFARI M. Thermal stress analysis of infinite anisotropic plate with elliptical hole under uniform heat flux [J]. Journal of Thermal Stresses, 2016, 39(11): 1341 − 1355. DOI: 10.1080/01495739.2016.1216038.
[28] CHAO C K, GAO B. Mixed boundary-value problems of two-dimensional anisotropic thermoelasticity with elliptic boundaries [J]. International Journal of Solids and Structures, 2001, 38(34−35): 5975−5994. DOI: 10.1016/S0020-7683(00)00403-0.
[29] WANG C, CHAO C. On perturbation solutions for nearly circular inclusion [J]. Journal of Applied Mechanics, 2002, 69: 36−44. DOI: https://doi.org/10.1115/1.1410367.
[30] JAFARI M, JAFARI M. Thermal stress analysis of orthotropic plate containing a rectangular hole using complex variable method [J]. European Journal of Mechanics-A/Solids, 2019, 73: 212 − 223. DOI: 10.1016/j. euromechsol.2018.08.001.
[31] JAFARI M, JAFARI M. Effect of hole geometry on the thermal stress analysis of perforated composite plate under uniform heat flux [J]. Journal of Composite Materials, 2019, 53(8): 1079−1095. DOI: 10.1177/0021998318795279.
[32] HERAKOVICH C T. Mechanics of fibrous composites [M]. Virginia: Johan Wiley & Sons, 1998.

(Edited by HE Yun-bin)

中文导读

热流作用下石墨/环氧复合材料层合板绝热多边形切口周围的热应力分布

摘要：本研究分析了在均匀热流下，影响参数对复合材料层合板多边形切口周围应力分布的影响。在经典层合板理论和二维热弹性分析的基础上，建立了分析方法。利用映射函数将带有圆形切口的对称穿孔层压板的解推广到多边形切口的解。研究了三角形、正方形和五角形切口对称复合材料层合板中切口角位置、钝度和宽高比、热通量角和层合板堆叠顺序等重要参数的影响。在绝热多边形切口的边缘采用诺伊曼边界条件。所研究层压板由石墨/环氧树脂(AS/3501)材料制成，具有$[30/45]_s$和$[30/0/-30]_s$两种不同的堆垛顺序。采用有限元结果验证了解析解的有效性。

关键词：解析解；热应力分析；多边形切口；复变法；聚合物复合材料